ENERGETIC PARTICLE SIGNATURES AT GAMMA-RAY, X-RAY AND RADIO WAVELENGTHS

N. Vilmer

LESIA, Observatoire de Paris, 5 Place Janssen, 92195-Meudon Cedex, France, nicole.vilmer@obspm.fr

ABSTRACT

Explosive phenomena of magnetic energy conversion in the solar corona lead to the production of energetic particles at all energies. Particles play a major role in the active Sun since they contain a large amount of the energy released during flares. I shall review here the available information on solar particle acceleration provided by X-ray/ γ-ray observations with peculiar emphasis on the results obtained recently by the Reuven Ramaty High Energy Solar Spectroscopic Imager (RHESSI) mission (Lin et al., 2002). Radio observations from mm to cm wavelengths provide complementary diagnostics on the spectra and number of energetic electrons. A new window has recently been opened with observations in the 200-400 GHz range. These observations reveal in some cases a new spectral component not yet completely understood.

1. INTRODUCTION

The Sun is a powerful particle accelerator. This has been known for years, since the first detection of solar energetic protons by ground-based neutron monitors, the first observations of gamma-ray line flares from energetic protons in 1972 and first detection of >100 MeV solar neutrons aboard SMM/GRS in 1982 (see e.g. Vilmer & MacKinnon, 2003 for a review). Radio observations of solar flares have also shown for a long time that the Sun is an efficient accelerator of deka-keV electrons, in association with active regions, even in the absence of flares.

Solar flares and coronal mass ejections (CMEs) are the most powerful events in the solar system. In several tens of minutes, they can convert up to 10^{32} ergs of magnetic energy into accelerated particles, heated plasma and ejected solar material. A new estimate of this energy budget has been performed by Emslie et al (2004a) based on the observations of ACE, RHESSI, SOHO, TRACE and WIND. It was e.g.shown that for the 23 July 2002 γ-ray line (GRL) flare observed by RHESSI, the energy contained in energetic electrons interacting at the Sun was comparable to the energy contained in interacting ions and comparable to the CME energy. Understanding particle acceleration in flares therefore provides powerful constraints on coronal energy conversion processes.

2. MULTI-WAVELENGTHS DIAGNOSTICS OF FLARE ENERGETIC PARTICLES

The most quantitative diagnostics of energetic particles interacting at the Sun are provided by hard X-ray/γ-ray observations which provide information on electron and ion energy spectra, numbers and energy contents. Complementary observations of the HXR bremsstrahlung emitting electrons are provided by the radio emission produced in the whole frequency range from 100 GHz to a few MHz. Radio emissions at metric/decimetric wavelengths (i.e. in the 100 MHz- 1 GHz range) most commonly produced by coherent plasma radiation mechanisms are a sensitive diagnostics of electrons of a few tens of keV injected upward and downwards in the corona from the acceleration site. Fig. 1a (from Aschwanden, 2002) shows one of the simple cartoon used to relate the particle acceleration site to the coronal energy release site and the respective locations of the radio and HXR emitting sites. The relationship between HXR and metric/decimetric radio emitting electrons has been studied since the 1980's, combining radio data with spectral or spatial resolutions and HXR spectra or images. More recently, comparisons of RHESSI HXR images and of radio emitting sites observed at several frequencies between 450 MHz and 164 MHz by the Nançay Radioheliograph have been performed (Vilmer et al., 2002; 2003, Pick et al., 2005, Dauphin et al., 2005). For one of the event, a very close correspondence between the change in the pattern of the HXR source in the 25-40 keV range and the pattern of the radio source at the highest imaged frequency (410 MHz) has been observed (Vilmer et al, 2002). This shows a causal relationship between the radio and HXR emitting sites which can be attributed to variations in the energy release and electron injection sites. Such variations of the radio emission in the development of X-ray flares had been described earlier (see e.g. Vilmer & MacKinnon, 2003 for a review) but the combination of RHESSI and NRH images provided the first direct comparisons between the evolution with time of HXR and radio sources. To directly probe the electron acceleration sites themselves, radio images in the 500 MHz-1 GHz are however clearly needed. The future new observing facility FASR (Frequency Agile Solar Radiotelescope) will observe in this frequency range and with no doubt bring major new constraints on the localization of the electron acceleration sites and the conditions in these sites.
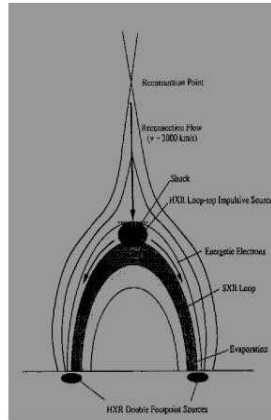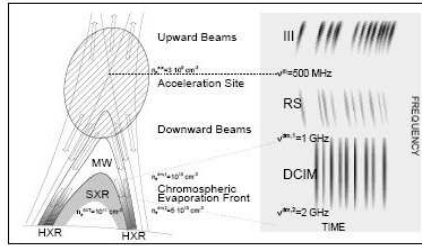
Figure 1: Cartoon scenarios for magnetic reconnection, particle acceleration and radiation emitting sites in solar flares (top from Aschwanden, 2002; bottom from Masuda et al., 1998).

Gyro-synchrotron emissions of energetic electrons from mm to cm wavelengths provide complementary diagnostics on the spectra and number of energetic electrons. This has led to many comparisons of HXR and mm/cm emitting electrons. A new window has recently been opened with observations in the 200-400 GHz range. Some of these results will be presented in Sect. 6.

3. HARD X-RAY AND γ-RAY DIAGNOSTICS OF ACCELERATED ELECTRONS AND IONS

Fig. 2 shows a theoretical HXR/GR spectrum of a solar flare from 1 keV to 100 MeV. Flare accelerated energetic electrons (energies above ≈ 10 keV) produce bremsstrahlung continuum emission by their braking in the Coulomb field of ambient ions, and above 500-700 keV of ambient electrons. This continuum is dominant below 1 MeV and again in the 10-50 MeV range. Energetic ions with energies in the ≈ 1 MeV/nuc to 100 MeV/nuc range produce through interaction in the solar atmosphere a complete γ-ray line spectrum which consists of several nuclear de-excitation lines, neutron capture and positron annihilation lines (see e.g. Ramaty,

1986). The temporal and spectral characteristics of HXR/GR and GRL radiations provide strong constraints on acceleration timescales, electron and proton energy spectra and numbers as well as energetic ion abundances. Figure 3 shows an example of the temporal evolution of HXR and GRL line emissions observed by RHESSI for the 23 July 2002 flare. The 2.2 MeV line from neutron capture radiation (3rd panel) is as expected delayed by ≈ 100 s with respect to the prompt γ-ray lines in the 3.2-6.5 MeV range (4th panel). This is due to the time needed for the thermalization of the fast neutrons produced in the nuclear reactions before they can be captured by ambient hydrogen to produce deuterium in an excited nuclear state leading to the emission of a 2.223 MeV photon.
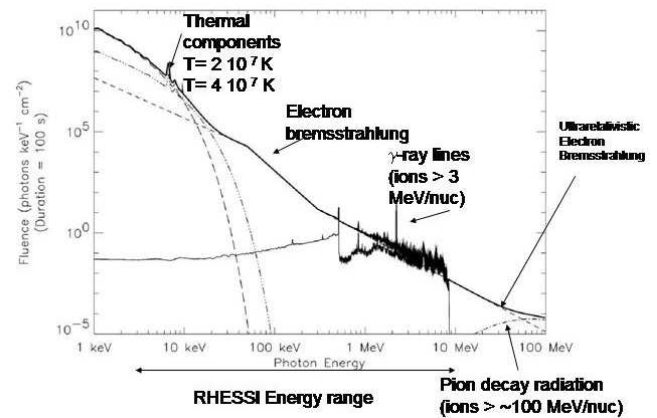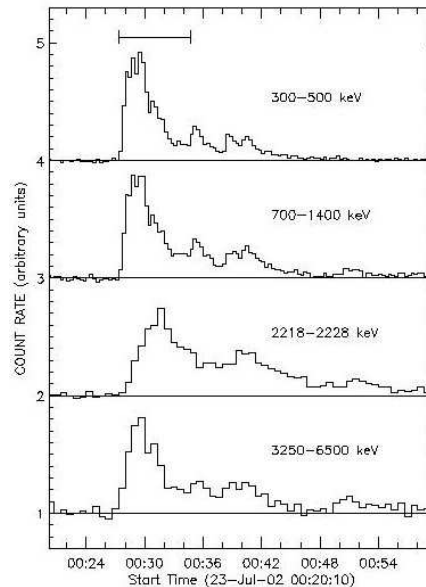

Figure 2: Theoretical HXR/GR spectrum

Figure 3: Background-subtracted light curves of the HXR/GRL flare observed by RHESSI in four energy bands (from Hurford et al., 2003).

Before the RHESSI launch, radiation above 100 keV was one of the last solar electromagnetic radiation where no spatially resolved observations were obtained. Quantitative constraints from HXR/GRL spectroscopy were also deduced from observations with limited spectral resolution. Finally the RHESSI experiment allows for the first time to make imaging spectroscopy of solar flares.

4. ENERGY RELEASE AND PARTICLE ACCELERATION SITES
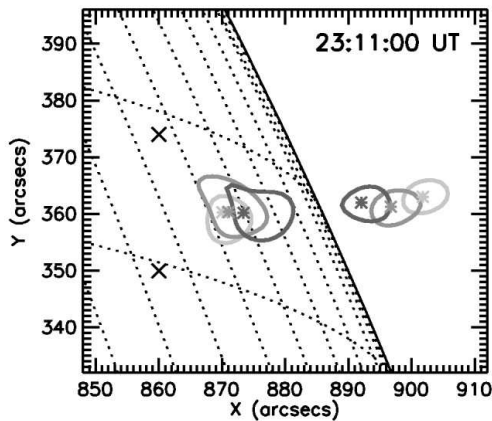
4.1 Evidence for current sheets

Figure 4:RHESSI images observed in different energy bands. The three contours (80% of the peak flux in each image) on the solar disk show the loop top sources in the following energy bands: 6-8 keV, 10-12 keV and 16-20 keV (from light to dark contours). The contours of the coronal sources aboce the limb are respectively for the 10-12, 12-14 and 14-16 keV energy bands (from light to dark). The crosses mark the two footpoints of the X-ray loop. (from Sui and Holman, 2003).

As suggested in Fig 1a, HXR (> 20 keV) images usually show double compact sources interpreted as footpoints of magnetic loops in which electrons propagate from the acceleration site before impinging on the chromosphere and producing thick-target X-ray emission. This was observed in most events with YOHKOH/HXT and confirmed by RHESSI observations. However, in a small number of events (<6), compact above the loop-top sources were observed in addition to double footpoint sources by YOHKOH/HXT (Masuda, 1994; Masuda et al., 1998). The above the loop-top sources were found to be located slightly at higher altitudes at higher X-ray energies and were interpreted as the result of the energization of the plasma by shocks originating from the reconnection site (see Fig. 1b). New evidence of loop top sources were found for three events with RHESSI observations (Sui et al., 2003; 2004) (Fig. 4). In addition to these loop-top sources, coronal sources are also observed with RHESSI at energies up to 20

keV. These coronal sources first stationary move upwards at 300 km/s after the main flare phase. More interestingly, while the temperature of the loop-top sources derived from the positions of thermal hard X-ray sources at different energies increases towards higher altitudes, the temperature of the coronal sources increases towards lower altitudes. These results are interpreted as indicating the formation of a current sheet between the top of the flare loops and the coronal source thus bringing new observational evidence for magnetic reconnection in flares.

4.2 Thick-target coronal sources

In some of the events, it is found that the corona can be dense enough to stop the non-thermal electrons thus leading to coronal thick-target hard X-ray non thermal sources (Veronig and Brown 2003), with little or no emission from the footpoints. The spectra of these coronal sources are furthermore shown to be consistent with steep ($\gamma \approx$-7) power-law spectra above 10 keV. Figure 5 shows another example of a thick target coronal source observed up to 25 keV for which the X-ray spectrum is a steep power law above 10 keV. These observations result from the emission of non-thermal electrons in a high enough density loop ($n > 10^{11}$ cm^{-3}), with a density which is consistent with the one deduced from the soft X-ray emission measure. The dense coronal loop acts as a collisional thick target even for electrons above 20 keV. The high loop density is furthermore found to be consistent with conductive evaporation driven by collisional healting at the loop top (Veronig and Brown, 2004).
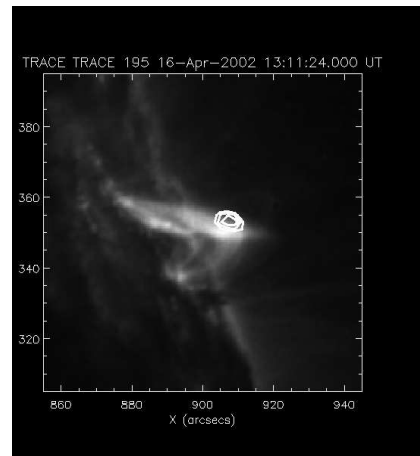

Figure 5: RHESSI contours at 12-25keV (60, 70, 80% of the peak flux) overlaid on a TRACE 195 A image.

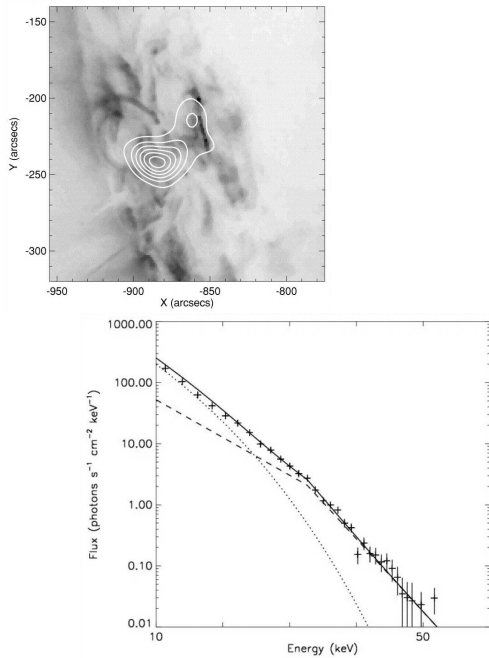## 4.3 Evolution in the flare of the energy release sites:

Figure 6: Top: RHESSI 12-30 keV image (15%, 30%, 45%, 60%, 75% and 90% contours) during the early phase of the 23 July 2002 GRL flare superposed on TRACE 195A image. Bottom: X-ray spectrum with a fit to isothermal (dotted line) and double power-law (dashed line) spectra and the sum (from Lin et al. 2003).

Fig 6 shows HXR images and spectra obtained in the early phase of the large 23 July 2003 GRL flare. The HXR emission above 10 keV is mostly produced in a coronal source with no chromospheric counterpart and the spectrum at that time clearly shows a non-thermal component at energies above 20 keV. From this combined image and spectrum it is found that an energy of at least 2 10^{31} ergs is already released in non-thermal electrons in this early phase, most of the energy contained in the electrons being deposited in the coronal source (Lin et al., 2003). As in the previous observations, this indicates that the electrons radiate in a dense enough loop acting as a chromospheric thick target. Later in the flare, the accelerated electron spectrum becomes much harder and the spatial configuration of the HXR sources evolves towards the common configuration showing HXR non thermal footpoints and a hot thermal coronal source. As in many other HXR flares, HXR source motions are observed in the course of the event (see e.g. Krucker et al., 2003). As seen in Fig. 7, an apparent motion of the northern footpoint and of the coronal source parallel to one of the flare ribbon is observed with a speed of 50 km/s in the flare impulsive phase. There is however no systematic motion of the southern footpoint. This is not in

agreement with simple reconnection models (e.g. Fig.1b) in which consistent motions of the two footpoints should be observed.
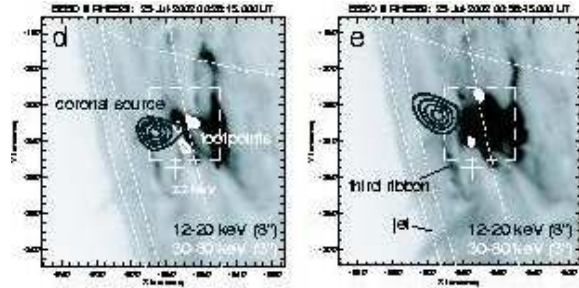

Figure 7: Location and evolution with time of the HXR sources observed at different energies during the main phase of the 23 July 2003 GRL flare. The black (12-20 keV) and white (30-80 keV) contours are resp. overlaid on BBSO Hα images (courtesy S. Krucker)

Furthermore, the motion is along the ribbons and not perpendicular to it. This indicates that the reconnection takes place in a highly sheared configuration. The absence of correlation between footpoint motions suggests that the 3D magnetic configuration connecting reconnection sites and footpoints is much more complex that the simple sketch drawn in figure 1. Other examples of apparent footpoint motions along ribbons have been observed with RHESSI (see e.g. Fletcher and Hudson, 2002; Grigis and Benz, 2005). On a more statistical basis, motions of HXR sources were systematically analysed for 72 flares of the YOHKOH/HXT data base (Bogachev et al, 2005). For 80 % of the flares, it was found that the apparent foot-point motion is more regular than chaotic. However, only a few % of the flares show foot-point motions away from and nearly perpendicular to the neutral line as would be expected from the simple cartoon of Fig. 1 if the reconnection site moves higher in the atmosphere as the flare progresses. For 26% of the flares, the foot-points move along the neutral lines in anti-parallel directions (such as shown in Fig. 8). Assuming that the HXR sources are the foot-points of newly reconnected loops, this antiparallel motion indicates that the reconnected field lines are highly sheared and that the shear angle changes as the flare evolves. In an even higher number of flares (35%), foot-point motions are found to be parallel along the neutral lines and in 26% of flares even more complicated foot-point motions are observed. These last observations therefore suggest as in the case of figure 7, a displacement of the particle acceleration region during the flare, consistent with what was suggested for many years the comparison of hard X-ray/γ-ray spectral measurements with metric/decimetric radio imaging observations (see e.g. Raoult at al., 1985; Trottet et al., 1998) and which has also led to the concept of the

complex flare (e.g. Vlahos et al. 1995). This last flare model, is based on the complexity of the magnetic topologies and the fragmentation of the magnetic energy release. In such a model, many current sheets of all scales are formed resulting from turbulent photospheric motions and leading to particle acceleration. In such models, motions of HXR sources are expected to be less systematic than in the simple cartoons shown above.
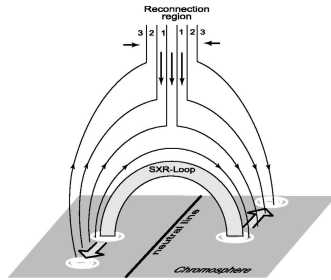

Figure 8:Evolution of the magnetic line reconnection (1-2-3) in a highly sheared magnetic configuration and associated HXR source motions (from Bogachev and Somov, 2005).

4.4 Electron and ion interaction sites

One of the most intriguing result from RHESSI imaging is the fact that in the first GRL event imaged (i.e. the 23 July 2002 event), the 2.2 MeV neutron capture line location was displaced by 20'' from the centroid of the HXR sources in the 50-100 keV range imaged in the same conditions (Fig.9) (Hurford et al., 2003). Although the 2.2 MeV line images the neutron interaction site rather than the energetic ion interaction site itself, it was nevertheless shown in Hurford et al. (2003) that the 2.2 MeV line emission locates the energetic ion interaction region within 1", thus still implying a previously unexpected significant displacement between the ion and electron interaction sites.

These different electron and ion interaction sites can be interpreted as revealing either different electron and ion acceleration sites or showing different transport for electrons and ions accelerated in the same site. One explanation was proposed so far by Emslie et al. 2004b based on the preferential acceleration of ions in large loops in the context of the electron and ion stochastic acceleration models based on cascading MHD turbulence (Miller, 2000). Fig. 10 shows indeed that the ratio of energetic electron and proton rates vary as a function of the length of the magnetic loops in which particles are accelerated through wave-particle interactions. Efficient acceleration of ions to high energies would indeed requires a lengthy period of interaction with the MHD turbulence and then larger loops. This could be an explanation for the further location of the ion interaction site from the HXR in the

case of the 23 July 2002 event. This interpretation has however some difficulties for the GRL event of 28 October 2003 event for which a similar displacement of 20 " of the HXR and 2.2 MeV sources is observed but for which similar separations are observed between the two HXR sources and the 2.2 MeV sources, therefore suggesting acceleration in loops of same size (Hurford, private communication).
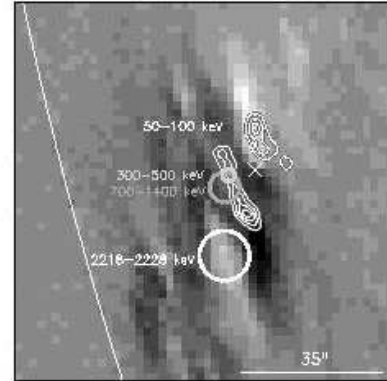

Figure 9: Locations of the HXR and GR sources for the 23 July 2002 GRL flare overlaid on a SOHO/MDI image. The circles represent the 1σ errors for the maps at different energies built in the same conditions with a 35" FWHM angular resolution. The white contours show with a resolution of 3" the HXR 50-100 keV footpoints and their evolution with time. The cross shows the centroid of the 50-100 keV source when imaged with the same resolution as the GRL source (i.e. 35") (from Hurford et al., 2003).
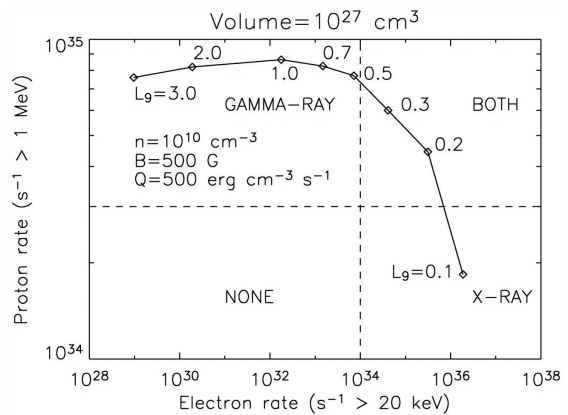

Figure 10: Acceleration rates for electrons (> 20 keV) and ions (> 1 MeV) as a function of the length of the acceleration region in the stochastic acceleration model of Miller (2000). L_g is the acceleration length in units of 10^9 cm (from Emslie et al., 2004b).

5. CONSTRAINTS ON ENERGETIC ELECTRONS AND IONS DEDUCED FROM HIGH RESOLUTION X/γ-RAY SPECTROSCOPY

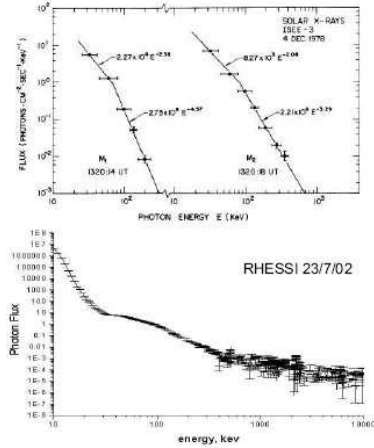## 5.1 Electron spectra and energy content

Figure 11: Comparison of HXR spectral resolution obtained with scintillators (top) and RHESSI Ge detectors (bottom) (from Brown and Kontar, 2005)

Fig. 11 (from Brown and Kontar, 2005) illustrates the dramatic changes in flare HXR spectroscopy provided by an increase in resolution from tens of keV with scintillators to around 1 keV with RHESSI Ge detectors. This enables detailed analysis of the bremsstrahlung continuum and resolution of individual γ-ray lines. The high resolution provided in the HXR domain allows a direct inversion of the bremsstrahlung photon spectrum to get the effective mean electron flux spectrum in the source (Brown et al., 2003; Piana et al. 2003) (Figs. 12 and 13). This quantity is the electron spectrum that would be required to observe the photon spectrum in a homogeneous source and is the only quantity which can be derived from the photon spectrum without making any assumption on the transport of electrons between acceleration and emitting sites. Fig. 13 shows the comparison of the values of the electron flux spectrum deduced by forward fitting of a model electron spectrum to the photon spectrum and of the regularized inverted spectrum. The agreement is quite good, given the high spectral resolution of RHESSI (Piana et al., 2003). The regularized inverted spectrum shows however a local minimum near 55 keV, which could not be determined from forward fitting. The interpretation of this local minimum is still under discussion but could be of potentially great importance in constraining acceleration mechanisms if it does not result from secondary effects such as photospheric back-scatter of the X-ray flux (i.e. albedo) (i.e. Alexander and Brown, 2002).
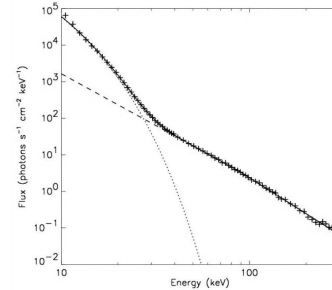

Figure 12: Example of RHESSI photon spectrum obtained in the impulsive phase of the 23 July 2002 GRL event. The dotted line represent the thermal component of the photon spectrum (T = 40 MK) and the dashed line represents the double power-law non-thermal spectrum (resp. -2.5 and -3.5 below and above 30 keV) (from Lin et al., 2003)
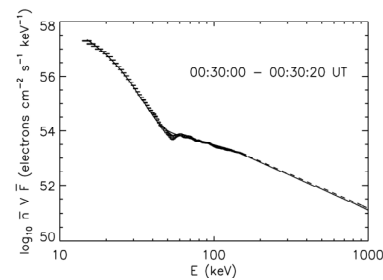

Figure 13: Regularized mean electron flux spectrum obtained from inversion of the photon spectrum (data points) observed by RHESSI in the impulsive part of the GRL 23 July 2002 event (Piana et al., 2003). The solid line shows the forward fitted electron spectrum necessary to reproduce the same X-ray spectrum (Holman et al, 2003).

Observations with high spectral resolution should also allow in principle to accurately separate the thermal and non thermal components of HXR spectra. This is quite crucial to be able to estimate the thermal and non thermal energy contents in a flare (see e.g. Vilmer & MacKinnon, 2003 for a discussion) since one of the important parameter is the low energy cut-off of the non thermal population (E_{lc}) (see Fig. 14). It is however a difficult task even with a highly resolved photon spectrum. It was shown indeed by Saint Hilaire and Benz (2005) that several fits can in fact lead to similar agreement between observed and modelled photon spectra depending on the shape of the electron spectrum which is assumed below the low energy cut-off (no electrons or a flat electron spectrum). The exact determination of the low–energy cut-off of the non thermal electron spectrum is however essential for studying the energy budget in flares since the largest fraction of the energy contained in non-thermal electrons comes in fact from electrons close to $E_{lc.}$ Several approaches are taken to try to solve this problem and to better constrain the relative contribution

of thermal and non thermal emissions. One consists in constraining the temperature of the thermal plasma by measuring the equivalent width of the broad Fe line at 6.7 keV formed for plasma temperatures >10 keV (Dennis et al., 2005), or by measuring the ratio of the Fe and Fe/Ni line fluxes (Caspi et al. 2004). Other possibilities to constrain E_{lc} come from the analysis of X-ray images at different energies assuming that observations of foot-points are an indication of a predominant non-thermal emission (Sui et al., 2005) or from the study of a "theoretical Neupert effect" (Veronig et al., 2005).
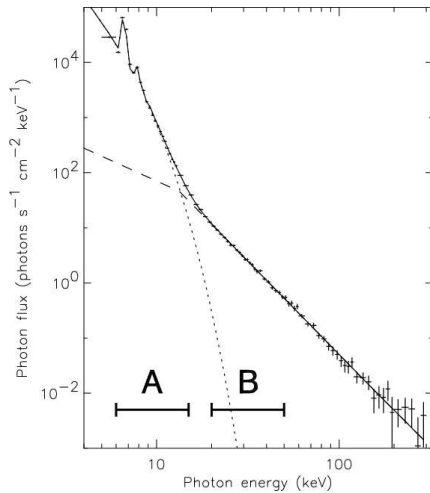

Figure 14: RHESSI photon spectrum from 4 keV to 300 keV (from Grigis and Benz, 2004). The dotted line shows the isothermal bremsstrahlung emission (T =17 MK). The dashed line shows the power-law non –thermal spectrum (γ~ -3.4) with a low energy turnover E_{lc}= 13 keV and a photon spectrum of -1.5 below E_{lc}. The two lines centered at 6.7 keV and 8 keV are broad lines from Fe and Fe/Ni formed for plasma temperatures > 10 MK.

Such an effect is derived from the Neupert effect which is the observed temporal correlation of the non-thermal HXR flux with the time derivative of the soft X-ray emission. This assumes that the energetic electrons which produce thick-target HXR emission are also the main sources of heating and mass supply of the SXR emitting coronal plasma. In that case a good correlation between the electron beam power above E_{lc} and the actual power needed to explain the SXR flux and spectrum must be found. This provides an additional constraint to determine E_{lc} and thus the non-thermal and thermal energy contents (Veronig et al., 2005). It is finally shown by Galloway et al. (2005) that a consistent treatment of accelerated and thermal electrons in the Fokker-Planck equation used to derive instantaneous electron spectra and therefore X-ray photon spectra should be used to better determine the total electron

energy. Indeed, when both the slowing-down and velocity diffusion of non-thermal electrons due to collisions in the corona are considered, the reduction of the low energy cut-off of non-thermal electrons is unexpectedly found to increase the relative magnitude of the thermal component of the spectrum, because the lowest energy electrons reach the background thermal distribution. This behaviour leads to surprising results in the sense that flares with apparently prominent thermal X-ray component extending photon energies above 20 keV may in fact have the lowest background plasma temperature and a large content of non-thermal electrons, the apparent thermal component of the photon spectrum being dominated by the thermalization of the numerous electrons accelerated at low energies. This of course considerably changes the partition between thermal and non-thermal energies, compared to the values which are usually found from the fitting of an iso-thermal and non-thermal power law components to the X-ray spectrum (Galloway et al., 2005).
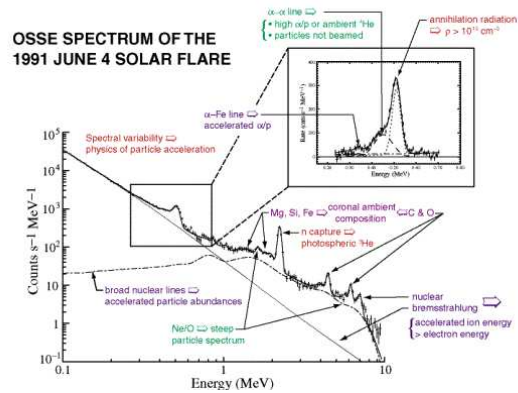
5.2 Ion spectra

Figure 15: OSSE HXR/GR spectrum of the large 4 June 1991 flare summarising the different components seen in the 0.1 to 10 MeV range (from Share and Murphy 2000).

Fig. 15 shows the complete γ-ray line spectrum observed with the OSSE detector aboard CGRO for the large 4 June 1991 solar flare. Strong deexcitation lines are found at 6.129 MeV from ^{16}O, 4.438 MeV from ^{12}C, 1.779 MeV from ^{28}Si, 1.634 MeV from ^{20}Ne , 1.369 MeV from ^{24}Mg and 0.847 MeV from ^{56}Fe. The nuclear deexcitation lines are either narrow or broad depending on whether they result from the bombardment of ambient nuclei by accelerated protons and α particles or from inverse reactions in which accelerated C or even heavier nuclei collide with ambient H or He. The broad lines merge in fact in a quasi continuum dominating the bremsstrahlung emission in the ≈1-8 MeV range. Deexcitation γ-ray lines provide information about ions

of energies above $\approx$1MeV/nuc. The energetic ion distribution below this energy is essentially unknown but still of particular interest for the total ion energy content. Since the first detection of γ-ray lines in 1972, quantitative results from γ-ray spectroscopy have been obtained for more than 20 events, yielding information on both atmospheric elemental abundances and on fast ion energy spectra. The threshold energies for excitation of Ne and O lines by fast protons are significantly different, $\approx$ 2 and $\approx$8 MeV respectively and the ratio of their measured fluxes can be used to infer the proton energy distribution (Share and Murphy, 1995). The spectrum deduced is then used to estimate the energy contained in energetic protons (Ramaty et al., 1995). The analysis based on these 20 events led to the conclusion that the energy contained in > 1MeV ions may be comparable to the energy contained in the sub-relativistic electrons and lie in the 10^{29} -10^{33} ergs for GRL flares. Of course, there is a large dispersion of the relative electron and ion energy contents from one flare to the other, the energy contained in the ions sometimes exceeding the energy in the electrons.
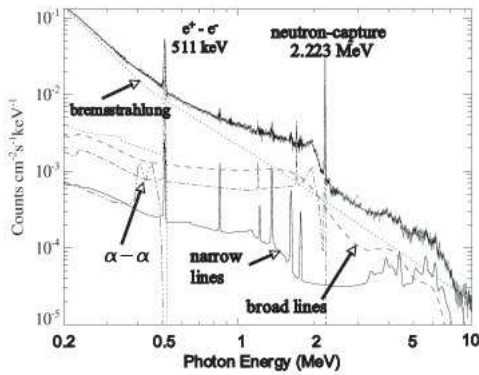

Figure 16: RHESSI spectrum recorded during the X17 flare on 28 October 2003. The spectrum shows the prominent neutron-capture line at 2.223 MeV, the positron annihilation line at 511 keV, the whole spectrum of narrow lines from accelerated protons and α's, the broad line component from accelerated heavy ions and features below 511 keV from α-α interactions. The bremsstrahlung continuum from accelerated electrons underlies the line features (from Share and Murphy, 2005)

So far, four γ-ray line events have been observed with high spectral resolution with RHESSI: 23 July 2002 (see Lin et al., 2003; Smith et al., 2003; Share et al., 2003), 28 October 2003 (Share et al., 2004); 2 November 2003 and 20 January 2005 (see Share and Murphy, 2005 for a review). RHESSI has for the first time the energy resolution necessary to resolve all the γ-ray lines, except the intrinsically narrow 2.223 MeV line, and to

determine the detailed line shapes expected from Doppler-shifts thus allowing to deduce velocity distributions of the interacting energetic ions (Smith et al., 2003). The comparison of fluxes in the ^{20}Ne line at 1.63 MeV and of the ^{12}C and ^{16}O lines at 4.44 and 6.13 MeV was performed for these four flares to provide information on the proton spectrum. Apart from the 23 July 2003 event for which the proton spectral slope was found to be $\approx$ -3.5 (Lin et al, 2003), the other events have a much harder slope (-2.2 to -2.5) (Share and Murphy, 2005). These four events are found to have much harder spectra than the average measured previously on the 19 SMM flares (-4.3).

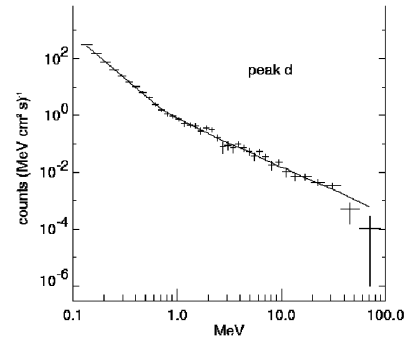## 6. A NEW OBSERVING WINDOW FOR HIGH ENERGY PARTICLES (100-200 GHZ SOLAR FLARE OBSERVATIONS)

Figure 17: Background subtracted HXR/GR spectrum observed by PHEBUS/GRANAT. The solid curve represents the fitted spectrum (from Trottet et al., 1998).

Complementary observations of HXR emitting energetic electrons are provided by the gyro-synchrotron emission that they produce in the low corona at cm/mm wavelengths. The relationship between the HXR and microwave emitting electrons has been studied for many years (see e.g. Vilmer & MacKinnon, 2003 for a review). In particular, the relationship between the spectral information deduced from HXR bremsstrahlung and from gyrosynchrotron emitting electrons has been found to be better understood when considering the spectral hardening of the X-ray continuum sometimes observed at energies above a few hundred keV (e.g. Fig. 17). It was indeed suggested by many authors that millimetre wave emission (at e.g. 90 GHz) is produced by high energy electrons (above or around 1 MeV) characterized by a spectrum much flatter than the one deduced deduced from X-ray observations around 100 keV (e.g. White and Kundu, 1992). The observed spectral hardening sometimes observed in flares strongly supports this suggestion. Furthermore, simple attempts to relate the spectral slopes of the bremsstrahlung and synchrotron emitting electrons for cases where observation in a wide

frequency range and a wide energy range are available, have shown that the centimetre/millimetre emitting electrons are related to the hard, high energy region of the HXR/GR spectrum (e.g. Trottet et al., 1998).

More recently, the first detection of impulsive radio emission at 212 GHz (Fig. 18) coupled with the observation of the gyrosynchrotron spectrum between a few GHz and 20 GHz has also shown that the very high frequency emission results from a population of ultra relativistic electrons with a hard energy spectrum (Trottet et al., 2002). Although the gyrosynchrotron emission is consistent with the radiation of electrons with a power law slope (- 2.7) and numbers consistent with what is observed for a middle -size X-ray event above 100 keV, the relationship between the electrons emitting at 212 GHz and any γ-ray emitting population remains an open question due to the lack of simultaneous, high-energy γ-ray observations.

Figure 18: Right: Time evolution of the 1.5-12 keV soft X-ray flux observed by GOES, the 15-30 keV and 120-240 keV HXR emission observed by INTERBALL, the 15.4 GHz measured by RSTN and the 212 GHz flux detected by SST. Left: Radio spectrum measured at the time of the impulsive HXR burst. The solid lines are theoretical spectra computed for magnetic fields of 300G, 500G and 700G and for a slope of -2.7 for the non-thermal electrons (from Trottet et al., 2002).

The opening of the new spectral window above 200 GHz for solar flares provided some unexpected observations for the two large X28 and X17 flares on November 4 2004 (Kaufmann et al., 2004) and October 28, 2003 (Lüthi et al., 2004). For these two flares, a new spectral component at high frequencies characterized by an increase of the radio flux at the highest frequencies has been observed. Its origin is not yet understood. The > 200 GHz emission may arise from optically–thick synchrotron emission from relativistic electrons in a source different from the one emitting at low frequencies, free-free emission from the chromosphere

due to energy deposited either by electrons and protons or by synchrotron emission from pion-decay positrons. This last process described a long time ago by Lingenfelter and Ramaty (1967) could be worthwhile reconsidering for these high frequency observations given that these two large flares also led to the production of very high energy radiation potentially from pion decay radiation observed by SONG on CORONAS-F (Myagkova et al, 2004).
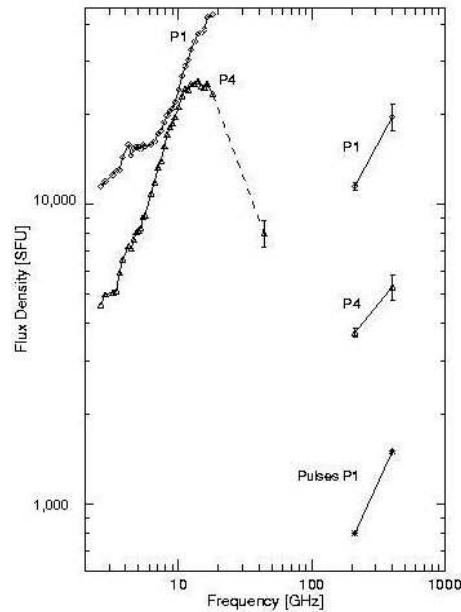

Figure 19: Spectra of bursts observed during the X28 November 4 2004 flare , showing a spectrum increasing with frequency from 212 to 405 GHz. Data points below 18 GHz and at 44 GHz are resp. from OVSO and Itapetinga. The data points at 212 and 405 GHz are from SST (Solar Submillimeter Telescope) (from Kaufmann et al., 2004).
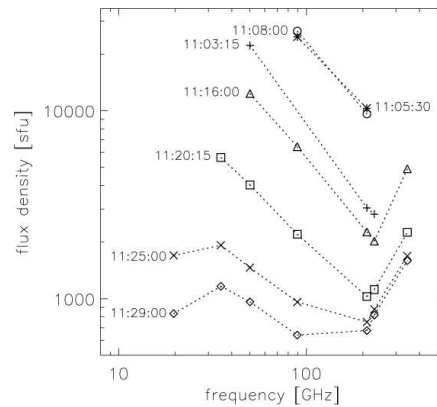

Figure 20: Temporal evolution of the radio spectrum between 19.6 and 345 GHz observed at Bern and Gornergrat (from Lüthi et al. 2005).

7. REFERENCES

Alexander R.C. and Brown J.C., *Solar Phys.,* Vol. 210, 407-418, 2002.

Aschwanden M.J., *Space Science Reviews,* Vol. 101, 1-227, 2002.

Bogachev S. Somov B.V. Kosugi T. and Sakao T., *ApJ,* Vol. 630, 561-572, 2005.

Brown J.C. Emslie A.G. and Kontar E.P., *ApJ,* Vol. 595, L115-L117, 2003.

Brown J.C. and Kontar E.P., *Adv Sp R,* Vol. 35, 1675-1682, 2005.

Caspi A. Krucker S. and Lin R.P., *COSPAR04 E2.3-0013-04,* 2004.

Dauphin C. Vilmer N. Lüthi T. et al., *Adv Sp R,* Vol.35, 1805-1812, 2005.

Dennis B.R. Phillips K.J.H. Sylwester J. et al., *Adv Sp R,* Vol. 35, 1723-1727, 2005.

Emslie A.G., Kucharek H., Dennis B.R. et al., *JGR,*Vol. 109, 104, 2004a.

Emslie A.G., Miller J.A., Brown, J.C., *ApJ,* Vol. 602, L69-L72, 2004b.

Fletcher L. and Hudson H.S., *Solar Phys.,* Vol. 210, 307-321, 2002.

Galloway R.K. MacKinnon A.L. Kontar E.P. and P. Helander, *A&A,* Vol. 438, 1107-1114, 2005.

Grigis P. and Benz A.O., *A&A,* Vol. 426, 1093-1101, 2004.

Grigis P. and Benz A.O., *ApJ*, Vol. 625, L143-L146, 2005.

Holmann G.D. Sui L Schwartz R.A. and Emslie A.G., *ApJ,* Vol. 595, L97-L101, 2003.

Hurford G.J. Schwartz R.A. Krucker S. et al., *ApJ,* Vol. 595, L77-L80, 2003.

Kaufmann P. Raulin J.P. de Castro C.G.G et al., *ApJ,* Vol. 603, L121-L124, 2004.

Krucker S. Hurford G.J. and Lin R.P., *ApJ,* Vol. 595, L103-L106, 2003.

Lin R.P. Dennis B.R. Hurford G.J. et al., *Solar Physics,* Vol. 210, 3-32, 2002.

Lin R.P. Krucker S. Hurford G.J. et al., *ApJ,* Vol. 595, L69-L76, 2003.

Lingenfelter R.E. and Ramaty R., *Planetary and Space Science,* Vol. 15, 1303, 1967.

Lüthi T. Lüdi A. and Magun A., *A&A,* Vol. 420, 361-370, 2004.

Masuda S., *Hard X-ray sources and the Primary Energy Release in Solar Flares,* PhD Tokyo, 1994.

Masuda S. Kosugi T. Sakao T. And Sato J., *Observational Plasma Astrophysics: Five years of YOHKOH and beyond,* 259, 1998.

Miller J.A., *Proceedings of IAU Symposium 195,* 277, 2000.

Myagkova I.N. Kuznetsov S.N. Yushkov B.Y. and Kudela K. , *COSPAR04 E2.30045-04,* 2004.

Pick M. Démoulin P. Krucker S. et al., *ApJ,* Vol.625, 1019-1026, 2005.

Piana M., Massone A.M., Kontar E.P. et al., *ApJ,* Vol. 595, L127-L130, 2003.

Ramaty R., *Physics of the Sun,* Vol. 2, 291-323, 1986.

Ramaty R. Mandzhavidze N. Kozlovsky B. et al., *ApJ,* Vol. 455, L193-L, 1995.

Raoult A. Pick M. Dennis B.R. and Kane S.R., *ApJ,* Vol. 299, 1027-1035, 1995.

Saint-Hilaire P. and Benz A.O., *A&A,* Vol. 435, 734-752, 2005.

Share G.H. and Murphy R.J., *ApJ,* Vol. 452, 933, 1995.

Share G.H and Murphy R.J., *ASP Conference Series,* Vol. 206, 377, 2000.

Share G.H. Murphy R.J. Smith D.M. et al., *ApJ,* Vol. 595, L89-L92, 2003.

Share G.H. Murphy R.J. Smith D.M. et al., *ApJ,* Vol. 615, L169-L172, 2004.

Share G.H. and Murphy R.J.,, *Solar Eruptions and Energetic Particles,* AGU monograph, 2004 Chapman Conference, 2004

Smith D.M. Share G.H. Murphy R.J. et al., *ApJ,* Vol. 595, L81-L84, 2005.

Sui L. and Holman G.D., *ApJ,* Vol. 596, L251-L254, 2003.

Sui L. Holman G.D. and Dennis B.R., *ApJ,* Vol. 612, 546-556, 2004.

Sui L. Holmann G.D. and Dennis B.R., *ApJ,* Vol. 626, 1102-1109, 2005.

Trottet G. Vilmer N. Barat C. et al., *A&A,* Vol. 334, 1099-1111, 1998.

Trottet G. Raulin J.P. Kaufmann P. et al., *A&A,* Vol. 381, 694-702, 2002.

Veronig A. and Brown J.C. , *ApJ,* Vol. 603, L117-L120, 2004

Veronig A. Brown J.C. Dennis B.R. et al., *ApJ,* Vol. 621, 482-497, 2005.

Vilmer N. Krucker S. Lin R.P. and the RHESSI Team, *Solar Physics,* Vol. 210, 261-272, 2002.

Vilmer N. Krucker S. Trottet G. and Lin R.P., *Adv Sp R,* Vol. 32, 2509-2515, 2003.

Vilmer N. and MacKinnon A.L., *Lecture Notes in Physics,* Vol. 612, 127-160, 2003.

Vlahos L. Georgoulis M. Kluiving R. and Paschos P., *A&A,* Vol. 299, 897, 1995.

White S.M. and Kundu M.R., *Solar Physics,* Vol. 141, 347-369, 1992.